Supporting Information to

Role of low-energy electrons in the solubility switch of Zn-based oxocluster photoresist for extreme ultraviolet lithography

Markus Rohdenburg[1,3], Neha Thakur[2], René Cartaya[1], Sonia Castellanos[2], Petra Swiderek[1*]

[1]Institute for Applied and Physical Chemistry (IAPC), Fachbereich 2 (Chemie/Biologie), University of Bremen, Leobener Str. 5 (NW2), 28359 Bremen, Germany
[2]Advanced Research Center for Nanolithography, Science Park 106, Amsterdam 1098 XG, The Netherlands
[3] Wilhelm-Ostwald-Institute for Physical and Theoretical Chemistry (WOI), Leipzig University, Linnéstr. 2, 04103 Leipzig, Germany

1. Estimate of relative product amounts in ESD

The relative amounts of the desorbing products as compared to CO_2 can be roughly estimated based on the intensities in the ESD data (Fig. 2). This estimate requires (i) a unique assignment of particular signals in the mass spectrum (MS) resulting from ESD to specific products, (ii) absolute ionization cross sections for these products at 70 eV, i.e., the energy used in the QMS, and (iii) knowledge of the fragmentation pattern of these products following ionization, i.e., of the MS.[1–3] On top of this, the mass discrimination of the quadrupole mass spectrometer (QMS) used in the present experiments must be taken into account. This residual gas analyser is tuned to enhance, in particular, low m/z ratios. Fig. S1 thus shows a comparison between the intensity distribution of signals obtained with the present QMS and the MS from the NIST database for n-octane as an example of a compound that exhibits signals in the m/z range relevant to the present study. The spectra are normalized to the signal at m/z 43 which is the strongest signal in the NIST spectrum and closest to the m/z 44 peak of CO_2 to which other desorbing species are compared when the ESD yields from Zn oxoclusters are analyzed. Table S1 summarizes correction factors for the intensities of specific m/z ratios that must be applied to compare the QMS data to MS data from NIST.
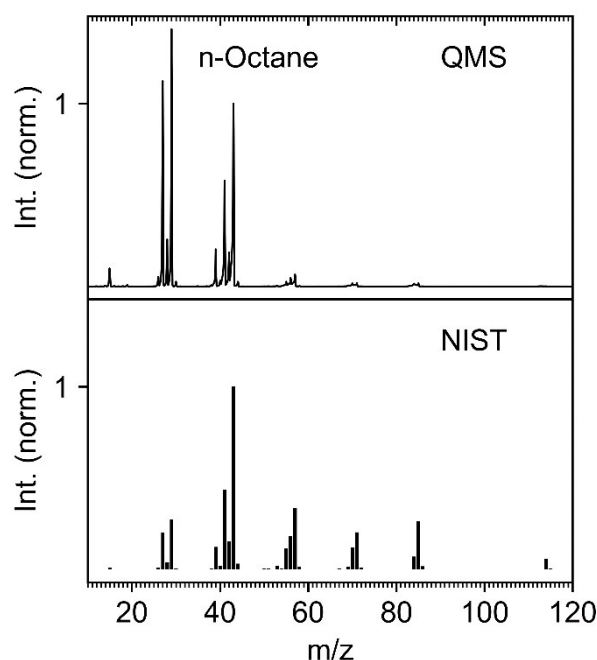

Fig. S1. MS of n-octane (C_8H_{18}) measured with the QMS used in this study (top) and from the NIST database.[4] Both spectra are normalized to the m/z 43 signal. The comparison reveals that the QMS used in the present experiments discriminates higher masses in favor of lower ones.

Table S1. Comparison of intensities for selected m/z signals in the MS of n-octane as obtained with the QMS used in this work to MS data retrieved from the NIST database.[4] The spectra are normalized to the m/z 43 signal.

m/z	Relative intensity obtained using QMS	Relative intensity according to NIST	Mass discrimination
15	9	0.9	10
29	138	27.4	5
41	57	43.8	1.3
43	100	100	1
57	7	33.5	0.2
70	2	12.1	0.17

The total ionization cross section of CO_2 and the partial ionization cross section for the parent ion at m/z 44 have been reported as 3.27 $Å^2$ and 2.13 $Å^2$.[5] Similarly, the total ionization cross section of H_2O is 1.99 $Å^2$ of which 1.27 $Å^2$ contribute as the partial ionization cross section for the parent ion at m/z 18.[5] Using these partial cross sections and considering that the contribution of other products to the signals at m/z 44 (CO_2) and m/z 18 (H_2O) is negligible, the relative amounts of H_2O and CO_2 that desorb during electron exposure from Zn(TFA) is derived from the relative peak heights in Fig. 2(a) as roughly 1:4. However, based on the mass discrimination effect of the QMS (see m/z 15 as closest signal in Figure S1 and Table S1), this must be corrected to roughly 1:30. A similar result can be derived from Fig. 2(b) for Zn(MA)(TFA).

The partial ionization cross section for the parent ion of the CF_3 radical has been reported as 0.376 $Å^2$ [6] and the partial ionization cross section for formation of CF_3^+ from CHF_3 as 0.813 $Å^2$.[7] Considering also mass discrimination, we deduce from the height of the m/z 69 signal in the case of Zn(TFA) as compared to m/z 44 (CO_2) (Fig. 2(a)) values of 1:5 ($CF_3:CO_2$) and 1:10 ($CHF_3:CO_2$) as an upper and lower limit for the relative yields of desorbing fluorinated products as compared to CO_2.

A partial ionization cross section for propene is used to estimate the amount of hydrocarbon products that desorb from the Zn(MA)(TFA) resist under electron irradiation (Fig. 2(b)). Based on a total ionization cross section of 8.736 $Å^2$ [10] and the relative intensities in the mass spectrum of propene,[6] we deduce a partial ionization cross section of 2.18 $Å^2$ for the dominant m/z 41 ($C_3H_5^{\cdot+}$) fragment of propene. From this we arrive at a relative yield of desorbing propene as compared to CO_2 of 1:50 (propene:CO_2).

Table S2. Estimate of relative product amount in ESD of Fig. 2 from representative peak heights using partial ionization cross sections (ics) reported in literature or derived as explained in text and including effect of mass discrimination.

	Zn(TFA), Zn(MA)(TFA)	Zn(TFA)			Zn(MA)(TFA)	
	$CO_2^{+\bullet}$ / CO2	$H_2O^{+\bullet}$ / H_2O	$CF_3^{+\bullet}$ / CF_3	$CF_3^{+\bullet}$ / CHF_3	$H_2O^{+\bullet}$ / H_2O	$C_3H_5^{+\bullet}$ / $CH_3CH=CH_2$
m/z	44	18	69	69	18	41
Relative Int.	100	19.4	0.65	0.65	15.7	2.5
Partial ics	2.13 Å^2 [5]	1.27 Å^2 [5]	0.376 Å^2 [6]	0.813 Å^2 [7]	1.27 Å^2 [5]	2.18 Å^2 [4,8]
Relative Int. / partial ics / Å^2	46.9	15.3[a]	1.7	0.8	12.4[a]	1.1
Mass discrimin. factor[b]	1	9	0.17	0.17	9	1.4
Relative amount	100	3.6	21	10	2.9	1.7

a Value to be considered as lower limit because ESD of H_2O decays more slowly than for other species.

b Estimated by interpolation between m/z values listed in Table S1.

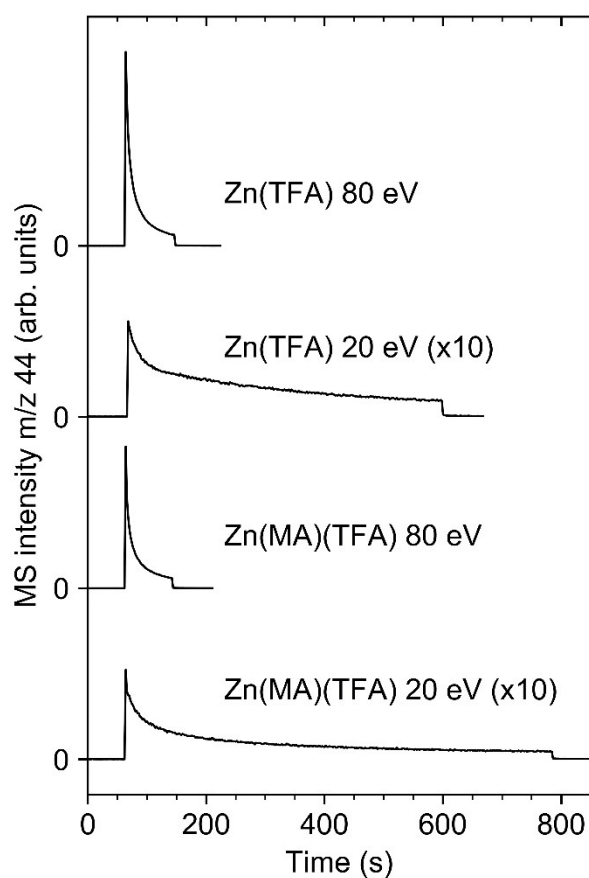## 2. Comparison of ESD of CO_2 at 80 eV and 20 eV

Fig. S2. Electron-stimulated desorption (ESD) of CO_2 from 14 nm Zn(TFA) resist layers and from 12 nm Zn(MA)(TFA) resist layers during an electron exposure of 2.5 mC/cm^2 at 80 eV and 20 eV. The sudden drop of the signal marks the end of irradiation. Sample currents during electron irradiation and integrated ESD intensities in arbitrary units (from top to bottom): 30 μA/cm^2 (area 3.39), 4.5 μA/cm^2 (area 1.89), 34.2 μA/cm^2 (area 2.41), 3.9 μA/cm^2 (area 1.33).

3. Vibrational bands of Zn(TFA) and Zn(MA)(TFA)

Table S3. Vibrational band positions (in cm^{-1}) observed in RAIRS of Zn(TFA) and Zn(MA)(TFA) resist layers and assignments.

Assignment	Zn(TFA)	Zn(MA)(TFA)	References
ν_{as}(TFA,CO$_2$)	1683	1682	[9,10]
ν(C=C)		1646	[10,11]
ν_{as}(MA,CO$_2$)		1595, 1569	[10,11]
ν_s(TFA,CO$_2$)	1456	1460	[9,10]
ν_s(MA,CO$_2$)+δ(CH$_2$)+δ(CH$_3$)		1427, 1375	[11]
ν(C-C)+ρ(=CH$_2$)		1244	[10,11]
ν_s(CF$_3$)	1223	1210	[9,10]
ν_{as}(CF$_3$)	1168	1156	[9,10]
ω(CH$_3$)		1009	[11]
ω(CH$_2$)		944	[11]
ν(TFA,CC)	853	850	[9]
CH$_2$ bending mode		825	[12]
δ(TFA,CO$_2$)	799	799	[9]
$\delta_{umbrella}$(CF$_3$)	735	729	[9]

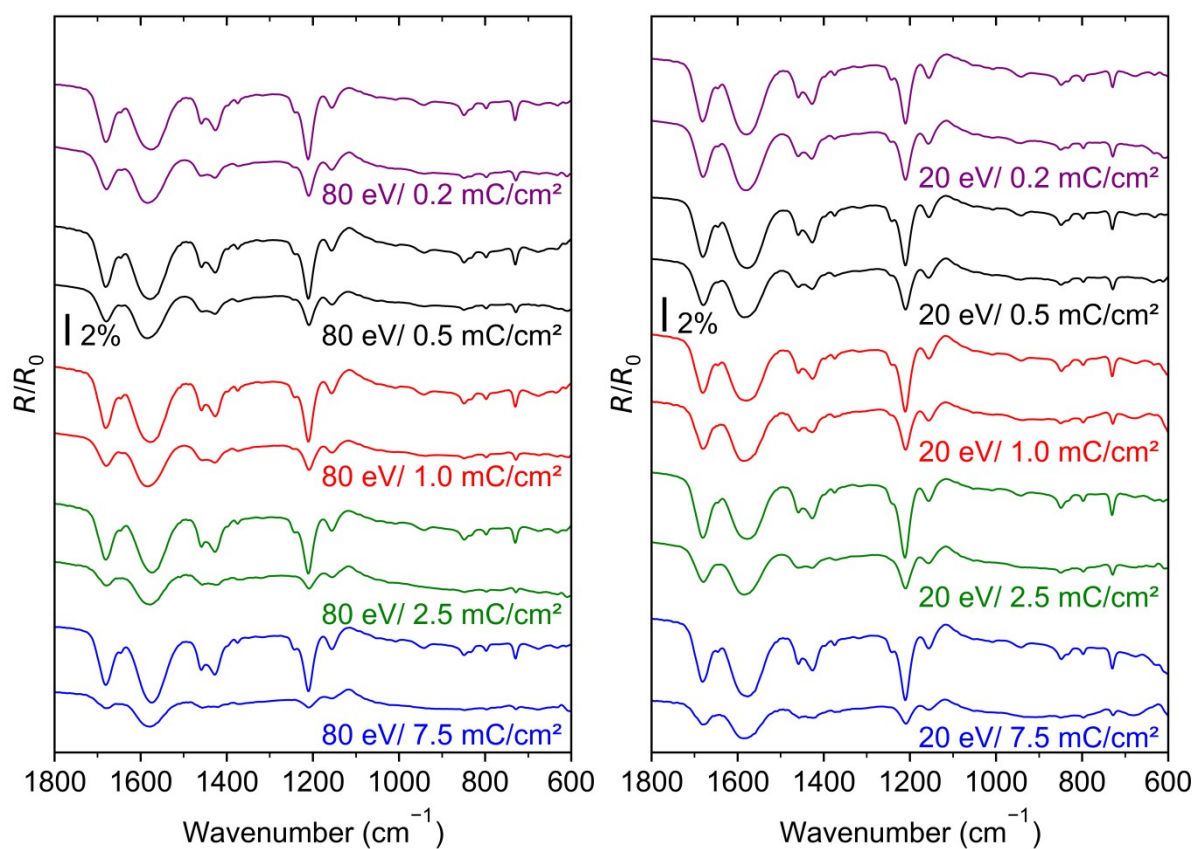## 4. RAIRS of Zn(TFA) and Zn(MA)(TFA) before and after electron irradiation

Fig. S3. RAIRS of 12 nm Zn(MA)TFA resist layers before (upper spectrum of each set) and after the stated electron exposures at 80 eV (left) and 20 eV (right).
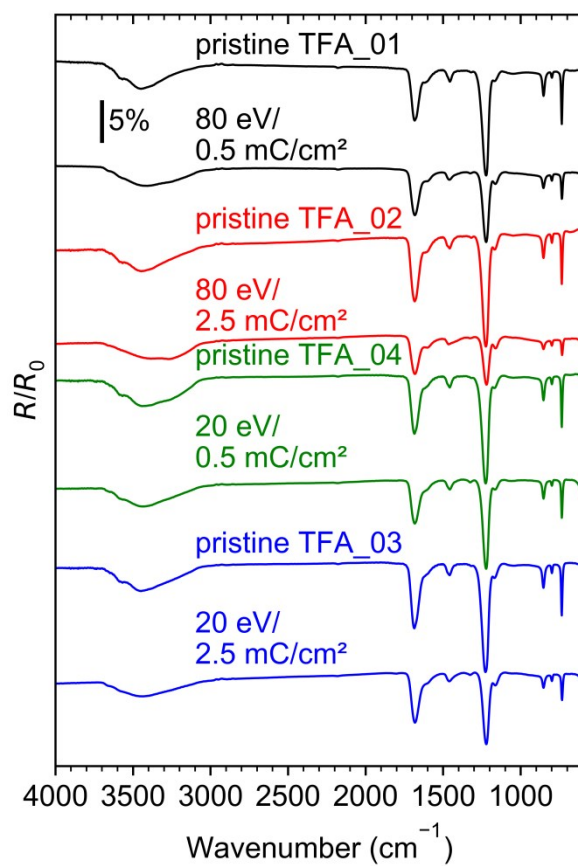
Fig. S4. RAIRS of 14 nm Zn(TFA) resist layers before (upper spectrum of each set) and after the stated electron exposures at 80 eV (top) and 20 eV (bottom).
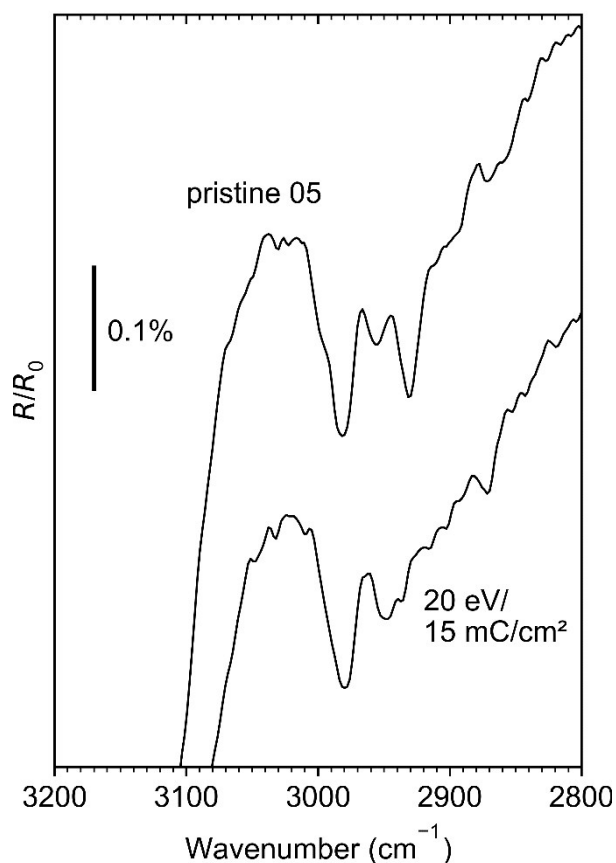
Fig. S5. C-H stretching spectral range of a 15nm Zn(MA)(TFA) resist layer before and after a 15 mC/cm² electron irradiation at 20 eV. Note that the bands are weak and sit on a background caused by formation of ice on the infrared detector thus ruling out their quantitative evaluation.
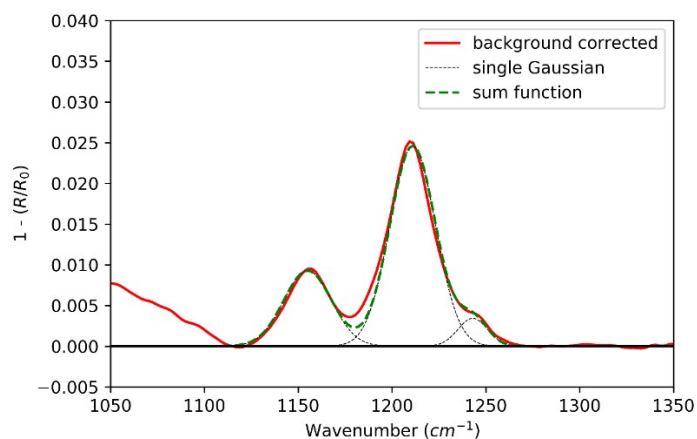

Fig. S6. Example of a fit of Gaussian functions to the characteristic TFA RAIRS bands $\nu_s(CF_3)$ (1223 cm^{-1}) and $\nu_{as}(CF_3)$ (1168 cm^{-1}) which, by integration of the Gaussians, together yields the overall ν(C-F) intensity as plotted in Fig. 7 of the main text. Equally shown here is the fit to the characteristic MA RAIRS band ν(C-C)+ρ(=CH$_2$) (1244 cm^{-1}).

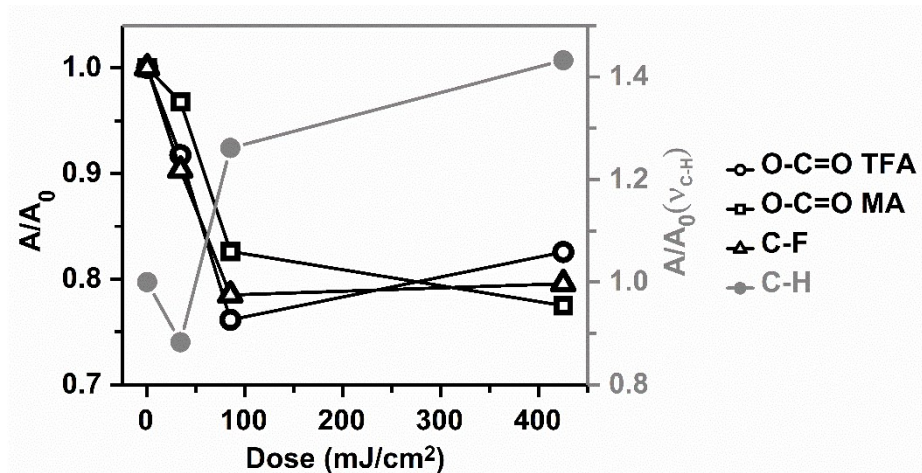## 5. Evolution of integrated infrared bands of Zn(MA)(TFA) with EUV dose

Fig. S7. Evolution of area of the characteristic band (A) relative to the unexposed (A$_o$, reference) of MA and TFA ligands in the FTIR spectra of Zn(MA)(TFA) thin film as a function of EUV dose: 34 mJ/cm^2, 85 mJ/cm^2 and 425 mJ/cm^2.[13]

References

1   T. Hamann, L. Kankate, E. Böhler, J. H. Bredehöft, F. M. Zhang, A. Gölzhäuser and P. Swiderek, Functionalization of a self-assembled monolayer driven by low-energy electron exposure, *Langmuir*, 2012, **28**, 367–376.

2   E. Böhler, J. H. Bredehöft and P. Swiderek, Low-energy electron-induced hydroamination reactions between different amines and olefins, *J. Phys. Chem. C*, 2014, **118**, 6922–6933.

3   F. Schmidt, P. Swiderek and J. H. Bredehöft, Formation of Formic Acid, Formaldehyde, and Carbon Dioxide by Electron-Induced Chemistry in Ices of Water and Carbon Monoxide, *ACS Earth Sp. Chem.*, 2019, **3**, 1974–1986.

4   W. E. Wallace, 'Mass Spectra' in NIST Chemistry WebBook, NIST Standard Reference Database Number 69, https://webbook.nist.gov/cgi/cbook.cgi?Contrib=MSDC, (accessed 1 October 2020).

5   J. W. McConkey, C. P. Malone, P. V. Johnson, C. Winstead, V. McKoy and I. Kanik, Electron impact dissociation of oxygen-containing molecules-A critical review, *Phys. Rep.*, 2008, **466**, 1–103.

6   V. Tarnovsky and K. Becker, Absolute partial cross sections for the parent ionization of the CF x (x=1-3) free radicals by electron impact, *J. Chem. Phys.*, 1993, **98**, 7868–7874.

7   I. Torres, R. Martínez and F. Castaño, Electron-impact dissociative ionization of fluoromethanes CHF3 and CF4, *J. Phys. B At. Mol. Opt. Phys.*, 2002, **35**, 2423–2436.

8   Y. K. Kim, K. K. Irikura, M. E. Rudd, M. A. Ali, P. M. Stone, J. Chang, J. S. Coursey, R. A.

Dragoset, A. R. Kishore, K. J. Olsen, A. M. Sansonetti, G. G. Wiersma, D. S. Zucker and M. A. Zukker, Electron-Impact Cross Sections for Ionization and Excitation Database, NIST Standard Reference Database 107, https://www.nist.gov/pml/electron-impact-cross-sections-ionization-and-excitation-database, (accessed 19 March 2021).

9   K. O. Christe and D. Naumann, Vibrational spectra of trifluoroacetates, *Spectrochim. Acta Part A Mol. Spectrosc.*, 1973, **29**, 2017–2024.

10   N. Thakur, L.-T. Tseng, M. Vockenhuber, Y. Ekinci and S. Castellanos, Stability studies on a sensitive EUV photoresist based on zinc metal oxoclusters, *J. Micro/Nanolithography, MEMS, MOEMS*, 2019, **18**, 43504.

11   J. Kreutzer, M. Puchberger, C. Artner and U. Schubert, Retention of the Cluster Core Structure during Ligand Exchange Reactions of Carboxylato-Substituted Metal Oxo Clusters, *Eur. J. Inorg. Chem.*, 2015, **2015**, 2145–2151.

12   E. C. Mattson, Y. Cabrera, S. M. Rupich, Y. Wang, K. A. Oyekan, T. J. Mustard, M. D. Halls, H. A. Bechtel, M. C. Martin and Y. J. Chabal, Chemical Modification Mechanisms in Hybrid Hafnium Oxo-methacrylate Nanocluster Photoresists for Extreme Ultraviolet Patterning, *Chem. Mater.*, 2018, **30**, 6192–6206.

13   N. Thakur, R. Bliem, I. Mochi, M. Vockenhuber, Y. Ekinci and S. Castellanos, Mixed-ligand zinc-oxoclusters: efficient chemistry for high resolution nanolithography, *J. Mater. Chem. C*, 2020, **8**, 14499–14506.